Solar Energy Materials & Solar Cells 92 (2008) 1621–1627

Contents lists available at ScienceDirect

Solar Energy Materials & Solar Cells

journal homepage: www.elsevier.com/locate/solmat

Note on the interpretation of electroluminescence images using their spectral information

Thomas Kirchartz [a,*], Anke Helbig [b], Uwe Rau [a]

[a] IEF5-Photovoltaik, Forschungszentrum Jülich, 52425 Jülich, Germany
[b] Institut für Physikalische Elektronik, Universität Stuttgart, 70569 Stuttgart, Germany

ARTICLE INFO

Article history:
Received 19 May 2008
Received in revised form
14 July 2008
Accepted 22 July 2008
Available online 30 August 2008

Keywords:
Luminescence
Reciprocity
LED
Quantum efficiency

ABSTRACT

We show how to use the reciprocity between electroluminescence and solar cell quantum efficiency for the simulation and interpretation of electroluminescence images. The analysis of the spectral properties of the electroluminescence images obtained by using different short- and long-pass filters yields information about surface recombination velocity, bulk diffusion length and reflection of the back side in flat and textured solar cells.

1. Introduction

Detecting the electroluminescent (EL) emission of a forward biased solar cell with a CCD camera [1–4] is a fast and simple method to obtain spatially resolved information about optical, resistive and recombinatorial effects in the device. A quantitative interpretation of EL images is hampered by the fact that the information contained in the image is a scalar for each position on the cell, regardless of the several unknown properties of the materials and of the solar cell, like series and shunt resistance, diffusion length, surface recombination or light-trapping efficiency. Würfel et al. [5] proposed to involve the spectral information of the EL emission by comparing two different EL images obtained using different filters. The contrast ratio between the two images finally yields the spatially resolved values of the diffusion length.

In order to better understand and exploit the method of Ref. [5] it is useful to remember the link between EL emission ϕ_{em} and the external solar cell quantum efficiency Q_e. A recently established reciprocity theorem connects both quantities via Ref. [6]

$$\phi_{em}(E,\mathbf{x}) = Q_e(E,\mathbf{x})\phi_{bb}(E)\left[\exp\left(\frac{qV(\mathbf{x})}{kT}\right) - 1\right], \quad (1)$$

where E is the photon energy, $\mathbf{x}$ is the surface position, ϕ_{bb} is the black-body radiation according to Planck's law, V is the local voltage drop across the rectifying junction and kT/q is the thermal voltage. Eq. (1) explains which quantities affect the spectral shape and the absolute amount of EL emission and why spectrally resolved EL measurements [7–9] are a useful tool for solar cell characterization.

With regard to the absolute intensity, the most powerful factor in Eq. (1) is the exponential voltage dependence. Since the local voltage $V(\mathbf{x})$ across the junction depends on the resistive losses across the emitter region of a pn-junction solar cell resistive losses often dominate the intensity distribution of EL images [3]. To asses the information provided by the external quantum efficiency term in Eq. (1) it is therefore necessary to eliminate the influence of $V(\mathbf{x})$ and to make use of the spectrum of the EL emission [5]. The interpretation of quantum efficiency data, however, is an old and well-established task for crystalline silicon photovoltaics [10,11].

In the following, we will therefore start with a short recapitulation of how to extract information from quantum efficiency measurements and then proceed to the case of EL measurements. The main purpose of this article is to provide the tools to simulate and thus interpret the spectral part of the EL emission. By comparing EL emission with the quantum efficiency, we show which information is contained in the different spectral parts of the EL. We discuss how and under which circumstances, electrical and optical parameters as well as recombination in the bulk and at the surface are distinguishable.

* Corresponding author. Tel.: +49 2461 613932; fax: +49 2461 613735.
E-mail address: t.kirchartz@fz-juelich.de (T. Kirchartz).

0927-0248/$ - see front matter © 2008 Elsevier B.V. All rights reserved.
doi:10.1016/j.solmat.2008.07.013

2. Interpretation of quantum efficiency data—a brief review

A method to extract diffusion lengths from quantum efficiencies was first proposed by Arora et al. [10] and later extended by Basore [11]. The general idea is to find a linear regime, where the slope of the curve is only proportional to the quantity of interest. In this case, the inverse internal quantum efficiency Q_i gives a straight line, when plotted versus the inverse absorption coefficient α, i.e. the absorption length $L_\alpha = \alpha^{-1}$. The internal quantum efficiency follows from the external by $Q_i = Q_e/(1-R_f)$, where R_f is the front surface reflectance. Fig. 1 shows an example of such a graph, where three sets of parameters have been used to simulate the internal quantum efficiency assuming a Lambertian front surface. As already discussed in detail by Basore [11], cells with good light trapping due to textured surfaces show two clearly distinguishable linear regimes. The first one for low absorption lengths $L_\alpha < w$, where w denotes the cell thickness, allows us to extract the effective diffusion length L_{eff} from the inverse slope. The relation between quantum efficiency and effective diffusion length for non-flat surfaces is

$$Q_i^{-1} = 1 + \frac{L_\alpha}{f_{\text{opt}} L_{\text{eff}}}, \tag{2}$$

where f_{opt} accounts for the average pathlength enhancement of the light on its first path through the device. For light, traveling under an angle θ to the surface normal, $f_{\text{opt}} = 1/(\cos(\theta))$ holds. Although Eq. (2) is only a useful approximation, the information that is usually accessible from the slope of the first linear region is indeed only the effective diffusion length

$$L_{\text{eff}} = L \frac{S \sinh(w/L) + D/L \cosh(w/L)}{S \cosh(w/L) + D/L \sinh(w/L)} \tag{3}$$

being an intimate mixture of bulk diffusion length L and surface recombination velocity S. Distinguishing between both is impossible with a single quantum efficiency measurement, however it is feasible to define lower and upper limits for both L and S [12].

The second linear regime for longer absorption lengths is heavily dependent on the optical properties of the device. Our example in Fig. 1 shows that already for absorption lengths L_α slightly below the cell thickness w, the data for different back surface reflectances R_b differ, although everything else is kept constant. However, Fig. 1 also shows that in the second linear regime Q_i is not independent of the recombination in the device, since for two different values for L and the same for R_b the result is different.

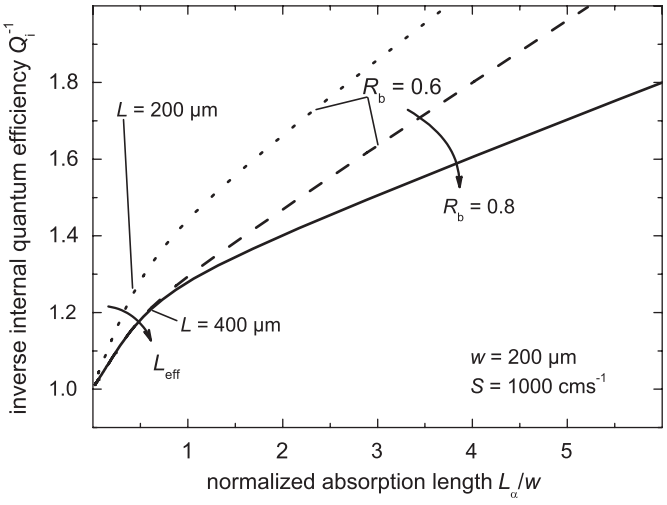

Fig. 1. Simulation of the inverse internal quantum efficiency of a textured crystalline silicon solar cell as a function of the normalized absorption length. The two linear regions yield information about the effective diffusion length (lower wavelengths and absorption lengths) and the back-side reflectance (higher wavelengths and absorption lengths).

With the connection between the quantum efficiency and the EL emission given by Eq. (1) and the results of our simulation in Fig. 1, we obtain two conclusions for the information contained in the spectral EL: first, a combination of S and L should be accessible from the high energy region without knowledge of R_b if we distinguish between flat and textured surfaces; second, information about the quality of light trapping should be accessible, possibly requiring some information about L and S.

3. Simulating electroluminescence spectra

A quantitative interpretation of the spectral component of the EL emission requires an accurate model of all unknown spectral parts of Eq. (1). Since the black-body spectrum

$$\phi_{\text{bb}}(E) = \frac{2\pi E^2/(h^3c^2)}{\exp(E/kT) - 1} \approx \frac{2\pi E^2}{h^3c^2} \exp\left\{\frac{-E}{kT}\right\} \tag{4}$$

is a known factor that depends basically on the photon energy, we only have to model the quantum efficiency and later multiply it by ϕ_{bb}. In Eq. (4), h is the Planck constant and c is the speed of light. To obtain the quantum efficiency one can either use device simulators like ASA, AFORS-HET or PC1D, which have been developed for use with solar cells, or apply analytical equations, which is feasible in pn-junction solar cells under low level injection. In the following, we will discuss these analytical equations, which were also used for all our simulations.

Modeling the quantum efficiency requires knowledge of the generation of charge carriers in the device as well as knowledge of the collection of photogenerated carriers. It is useful to write the internal quantum efficiency Q_i as a function of generation rate $g(x)$ and collection efficiency $f_c(x)$ as

$$Q_i(E) = \int_0^w g(x) f_c(x)\, dx, \tag{5}$$

where the generation rate $g(x)$ is defined normalized to the photon flux entering the cell; i.e. for the simplest case of flat surfaces and no back reflections $g(x) = \alpha \exp(-\alpha x)$.

Eq. (1) is valid for the case of low-level injection, where minorities can be clearly defined. The validity of Eq. (1) requires the validity of the Donolato theorem [13] relating the collection efficiency $f_c(x)$ of photogenerated carriers with the normalized dark carrier concentration. Thus, we obtain the collection efficiency from the solution of the diffusion equation for minorities in the dark as

$$f_c(x) = \cosh(x/L) - \frac{L}{L_{\text{eff}}} \sinh(x/L). \tag{6}$$

The calculation of the generation rate $g(x)$ depends on the optical properties of the device. For flat surfaces and multiple reflections at front and back surface, the generation rate is

$$g(x) = \frac{\alpha(1-R_f)(e^{-\alpha x} + R_b e^{\alpha(x-2w)})}{1 - R_f R_b e^{-2\alpha w}}. \tag{7}$$

For textured surfaces, the generation rate is either calculated with a ray-tracing program or the texture is approximated with perfectly Lambertian surfaces. An analytical solution of the generation in a cell with a Lambertian front surface and a specular back surface follows from Ref. [14] as

$$g(x) = 2\alpha(1-R_f) \frac{[\text{Ei}_2(\alpha x) + R_b \text{Ei}_2(\alpha(2w-x))]}{1 - t_{\text{cell}}(1 - t_{\text{lamb}})} \tag{8}$$

with $t_{lamb} = (1-R_f)/n^2$, where n is the index of refraction. Eq. (7) uses the definition

$$t_{cell} = R_b(e^{-2\alpha w}(1 - 2\alpha w) + (2\alpha w)^2 \mathrm{Ei}(2\alpha w)) \quad (9)$$

for the angle-integrated transmission of the cell from the front with one reflection at the back side to the front, where

$$\mathrm{Ei}(z) := \int_z^\infty \frac{e^{-t}}{t}\,dt \quad (10)$$

is the exponential integral, and

$$\mathrm{Ei}_2(z) := z\int_z^\infty \frac{e^{-t}}{t^2}\,dt = e^{-z} - z\mathrm{Ei}(z). \quad (11)$$

4. Results and discussion

As already mentioned, the spectral shape of the EL emission depends on both recombination in bulk and interfaces as well as the optical properties of the device. First, we will only concentrate on recombination and assume the optical properties to be known. In a second step, we will show how to distinguish between both optical and electrical properties. For all cases, we will concentrate on the following relevant parameters: bulk diffusion length L, surface recombination velocity S of the back side, reflection coefficient R_b of the back side and thickness w of the base, which is assumed to be identical to the total optical thickness. For simplicity, we assume for all simulations that the front side reflectance is zero for all wavelengths and, thus, do no longer distinguish between internal and external quantum efficiency. In the following, we will thus speak of the quantum efficiency $Q = Q_i = Q_e$. For interpretation of real measurements, the front side reflectance has to be measured separately and must be taken into account for simulations.

Fig. 2 shows the simulated quantum efficiency and EL for different values of the bulk diffusion length $L = 50$, 100, 200, 300, 400 and 800 μm, respectively. The other parameters used are $S = 1000$ cm/s, $w = 200$ μm, $R_b = 0.8$. The curves for the EL follow from the application of Eq. (1), i.e. the quantum efficiencies are first multiplied by the black-body spectrum and then normalized to the peak for the highest diffusion length. Like in Fig. 1, we see a wavelength dependence of the influence the diffusion length has on both Q and EL. We also notice the dramatic decrease of EL intensity for the shorter wavelengths. For instance around 900 nm, where the quantum efficiency is usually evaluated to extract the effective diffusion length, the total intensity is around four orders of magnitude below the peak. Using the spectral information in the low wavelength regime will thus always have the downside of longer data acquisition times.

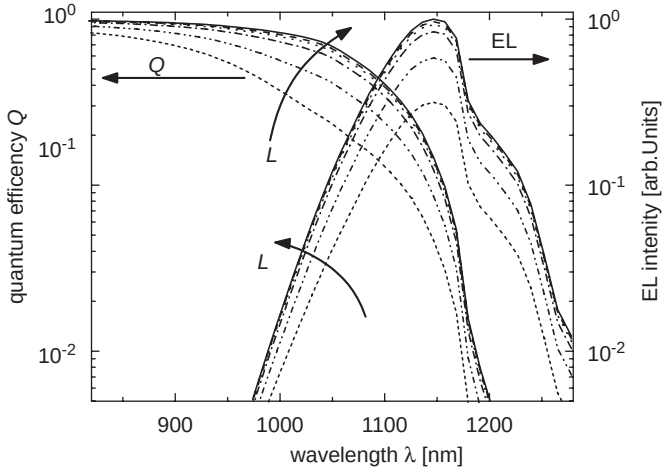

Fig. 2. Simulation of quantum efficiency and electroluminescence versus wavelength for different values of the bulk diffusion length $L = 50$, 100, 200, 300, 400 and 800 μm.

To access the spectral information with a camera, we have to use a limited number of filters and evaluate the contrast of measurements with and without a certain filter or combination of filters. We define the contrast C_s obtained from the ratio of two images taken with different step-function like *short-pass* filters as

$$C_s\left(E_{cut,1} = \frac{hc}{\lambda_{cut,1}}, E_{cut,2} = \frac{hc}{\lambda_{cut,2}}\right) = \frac{\int_{hc/\lambda_{cut,2}}^{\infty} \phi_{em} Q_{CCD}\,dE}{\int_{hc/\lambda_{cut,1}}^{\infty} \phi_{em} Q_{CCD}\,dE}, \quad (12)$$

where Q_{CCD} is the sensitivity of the camera and $\lambda_{cut,i}$ is the cut wavelength for the ith filter.

Fig. 3 shows how the information about the different diffusion lengths influences the contrast as defined in Eq. (11). Fig. 3a depicts the EL spectra of the highest—$L = 800$ μm and lowest—$L = 50$ μm diffusion length from Fig. 2 but now normalized to their respective peaks. The spectrum for $L = 800$ μm (solid line) has a steeper slope on the low wavelength side than the spectrum for $L = 50$ μm (dashed lines). It is this difference in slope that we want to detect with a filter. The absolute difference between the

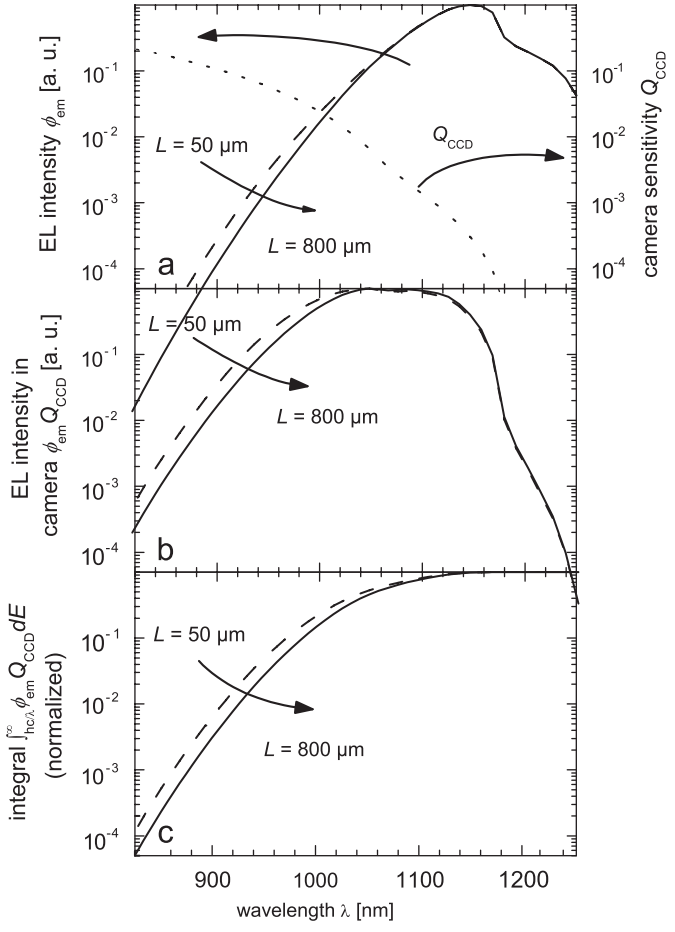

Fig. 3. (a) EL spectra for the diffusion lengths $L = 50$ μm (dashed line) and $L = 800$ μm (solid line), both normalized to their respective peak. The relative difference in slope on the short wavelength side needs to be detected by the use of filters. Camera sensitivity as a function of wavelength (dotted line). (b) Multiplication of EL spectra with the camera sensitivity. (c) Integration of EL spectra in (b) from short wavelengths up to the cut wavelength of a filter as a function of this cut wavelength. The result is normalized to the integral over the total spectrum (without filter), and thus the normalized integral approaches unity for high wavelengths. The filter is assumed to have a step-function-like transmission (i.e. all wavelengths $\lambda \leqslant \lambda_{cut}$ pass the filter).

curves with different diffusion lengths, which was depicted in Fig. 2, cannot be used, since it affects the absolute EL emission just like changes in voltage. In addition, Fig. 3a shows the camera sensitivity, which is taken from Ref. [15] and extrapolated with an absorptance of flat crystalline silicon to have data also for longer wavelengths.

However, it is not the EL spectrum in Fig. 3a that determines the output of the camera, but instead the multiplication of the spectra in Fig. 3a with the camera sensitivity Q_{CCD} in the same figure. Fig. 3b shows the result of this multiplication. Due to the decreased camera sensitivity for long wavelengths, the resulting spectra pronounce the short wavelength part stronger compared to the original spectra.

If we now introduce a short-pass filter with cut wavelength λ_{cut}, the actual signal of the camera, will be the integral $\int_{hc/cut}^{\infty} \phi_{em} Q_{CCD}\, dE$. Fig. 3c shows this integral as a function of cut wavelength normalized to the integral over the whole spectrum from Fig. 3b. According to the definition of the contrast in Eq. (11), the curves in Fig. 3c are equivalent to the inverse contrast for the case where one short-pass filter is used for the first image and the other image is taken without filters, i.e. for the case $C_s(hc/\lambda_{cut,l},0)$. Note here that the contrast is defined in a way that it is always larger than one and thus in the same way as in Ref. [5].

Fig. 4a shows the contrast $C_s(hc/\lambda_{cut,l},0)$ as a function of the cut wavelength $\lambda_{cut,l}$ for the EL spectra in Fig. 2. The most obvious result of Fig. 4a is the steep increase of the absolute contrast for decreasing wavelength. This implies that the denominator of Eq. (11) becomes very small for short cut wavelengths, and thus the signal to noise ratio for the filtered image becomes very low. However, we are not interested in the absolute contrast C_s but instead in the relative change in contrast induced by the change in diffusion length.

In order to better highlight these relative changes, we introduce the normalized contrast C_{sn}. Fig. 4b shows C_{sn}, normalized to the absolute contrast of the cell with the highest diffusion length $L = 800\,\mu m$. The normalized contrast is more sensitive to changes in diffusion length, when the cut wavelength gets shorter; i.e. a compromise must be made between signal to noise ratio and selectivity.

The right choice of the cut wavelength will depend on the signal to noise ratio and the tolerable duration of the measurement. A shorter measurement time with a filter with a higher cut wavelength will lead to less accuracy in the determination of the recombination parameters. Thus, we cannot give a general answer to the question for the perfect filter wavelength; however, we show how to estimate or simulate the effects, which may help to find the optimal filter for a given sample and setup.

Now, we will consider two unknowns, the bulk diffusion length and the back-side reflection and assume a Lambertian generation profile. We choose a matrix of two bulk diffusion lengths $L = 200$ and $400\,\mu m$ as well as two back-side reflections $R_b = 0.6$ and 0.8, while keeping $S = 1000\,cm/s$ and the thickness $w = 200\,\mu m$ constant. Fig. 5a shows the corresponding situation for the normalized contrast with only *one short-pass* filter. Fig. 5a clearly reveals that it is very challenging to distinguish between optics and recombination with only one filter.

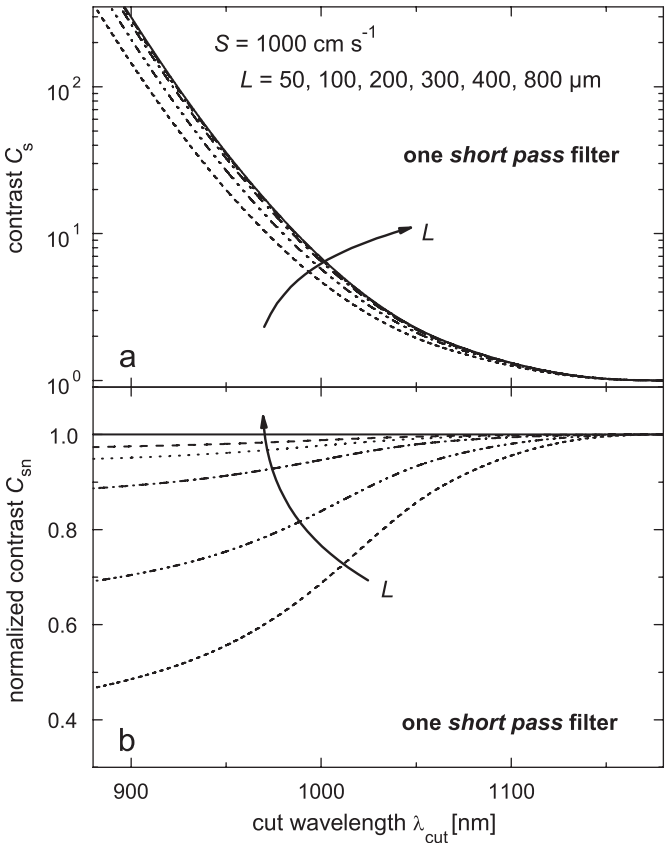

Fig. 4. Simulation of (a) contrast and (b) normalized contrast of two images, where one is taken without filter and the other with a short-pass filter with a cut wavelength λ_{cut}. The filter is assumed to have a step-function-like transmission (i.e. all wavelengths $\lambda \leqslant \lambda_{cut}$ pass the filter). Parameters are a diffusion length $L = 50$, 100, 200, 300, 400 and $800\,\mu m$, a surface recombination velocity $S = 1000\,cm/s$, a back reflectance $R_b = 0.8$ and a thickness $w = 200\,\mu m$.

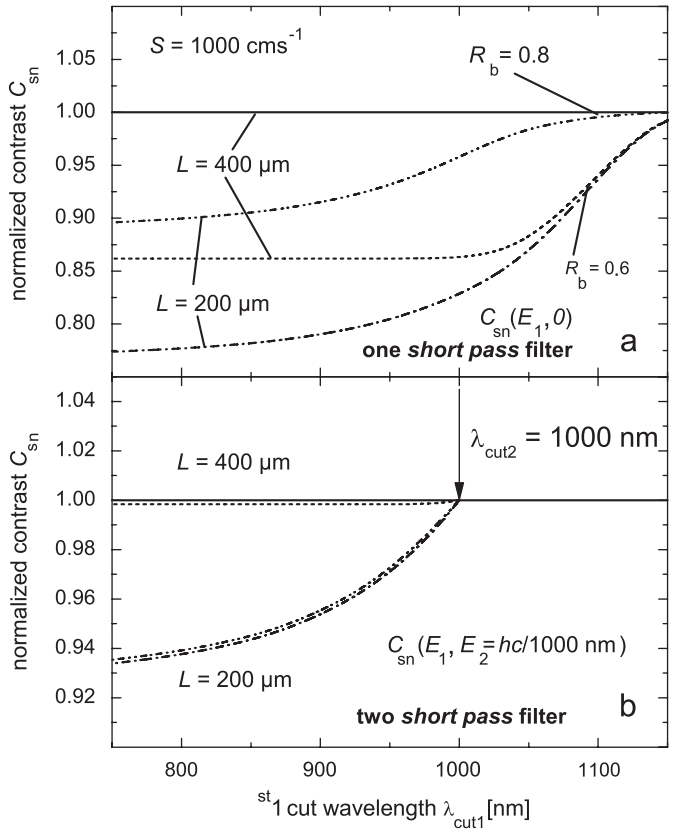

Fig. 5. Normalized contrast for the case of variable diffusion length L and back-side reflectance R_b for the case of (a) one short-pass filter or (b) two short-pass filters with the higher wavelength filter being used for both measurements. The effect of the second filter makes the result nearly independent of the back-side reflectance. Parameters are a diffusion length $L = 200$ and $400\,\mu m$, a back reflectance $R_b = 0.6$ and 0.8, a surface recombination velocity $S = 1000\,cm/s$ and a thickness $w = 200\,\mu m$.

This situation greatly improves if we follow the scheme of Ref. [5] and use a second short-pass filter around 1000 nm for the measurement that was done without filter before. Fig. 5b shows this situation for a variable value of the first cut wavelength, keeping the cut wavelength of the second filter constant at 1000 nm. The effect of the different back-side reflections vanishes. However, the selectivity—i.e. the change in normalized contrast between two diffusion lengths—decreases considerably with the introduction of the second filter.

Thus, we again have the need to make a compromise in choosing the second filter. The cut wavelength should be high enough for a good contrast and low enough for a sufficient suppression of light-trapping effects. The value $\lambda_{cut} = 1000$ nm, which is chosen here, corresponds to a penetration depth L_α roughly 1.3 times the cell thickness w. Simulations with other cell thicknesses and reflection coefficients R_b showed that a value of $L_\alpha/w = 1$–1.5 is quite reasonable for a wide range of thicknesses and nearly independent of the value of R_b.

Since we are able to simulate the EL emission for all wavelengths, we also try to exploit any information about light trapping, contained in the spectrum. For this purpose, it is helpful to choose *long-pass* filters, instead of *short-pass* filters. We define the contrast C_l obtained from the ratio of two images, where one is taken with a *long-pass* filter as

$$C_l\left(E_{cut} = \frac{hc}{\lambda_{cut,l}}\right) = \frac{\int_0^\infty \phi_{em} Q_{CCD}\, dE}{\int_0^{hc/\lambda_{cut}} \phi_{em} Q_{CCD}\, dE}, \quad (13)$$

where λ_{cut} is the cut wavelength for the long-pass filter.

How does the contrast C_l give information about the light trapping? To answer this question, we again go step-by-step from the spectra to the contrast. Fig. 6a shows EL spectra for two back reflectances $R_b = 0.6$ (dashed line) and $R_b = 0.8$ (solid line). The other parameters are $L = 400$ μm, $S = 1000$ cm/s and the thickness $w = 200$ μm. In contrast to Fig. 3a the spectra are now not normalized to the peak.

Multiplication of the spectra in Fig. 6a with the camera sensitivity in Fig. 6a gives the spectra in Fig. 6b that control the camera signal. It is obvious that the difference between the two spectra with difference back side reflectances affects the spectra on their high wavelength sides. Thus, in order to detect these differences with a filter, we need to choose filters with higher wavelengths and inverse behaviour, i.e. long-pass filters.

Fig. 6c shows the result of solving the integral $\int_0^{hc/\lambda_{cut}} \phi_{em} Q_{CCD}\, dE$ as a function of λ_{cut} and normalizing it to the integral over the whole spectrum. It is obvious that the differences between the spectra in Fig. 6b are still visible after the integration carried out by the camera pixels if a long-pass filter with cut wavelengths above 1000 nm is used. The inverse of the spectra in Fig. 6c gives the contrast C_l (not shown) and from that the normalized contrast follows in the same way as for short-pass filters.

Fig. 7 shows this normalized contrast for the four parameter combinations also used in Fig. 5: $R_b = 0.6$ and 0.8 and $L = 200$ and 400 μm. Since, we have defined the contrast in a way that it is always larger than one, the curve with high R_b and L is now at the bottom and a decreasing quality of light trapping, i.e. a smaller R_b, leads to higher absolute contrast. The difference between $R_b = 0.6$ and 0.8 becomes pronounced already at cut wavelengths $\lambda_{cut} = 1050$ nm, which is around the typical peak position in detected emission of Si CCD cameras. Thus, the evaluation of light trapping will not require long data-acquisition times.

Up to now, we only considered variations of the bulk diffusion length and back-side reflection. However, as for the quantum efficiency, the effects of surface and bulk recombination are closely intermixed. Thus, Fig. 8 shows the meaning of the absolute contrast $C_s(hc/\lambda_{cut,l},0)$ for the example of one short-pass filter with the cut wavelength $\lambda_{cut} = 900$ nm in terms of possible combinations of surface recombination velocity S and bulk diffusion length L leading to the same contrast value. It is obvious that rather large

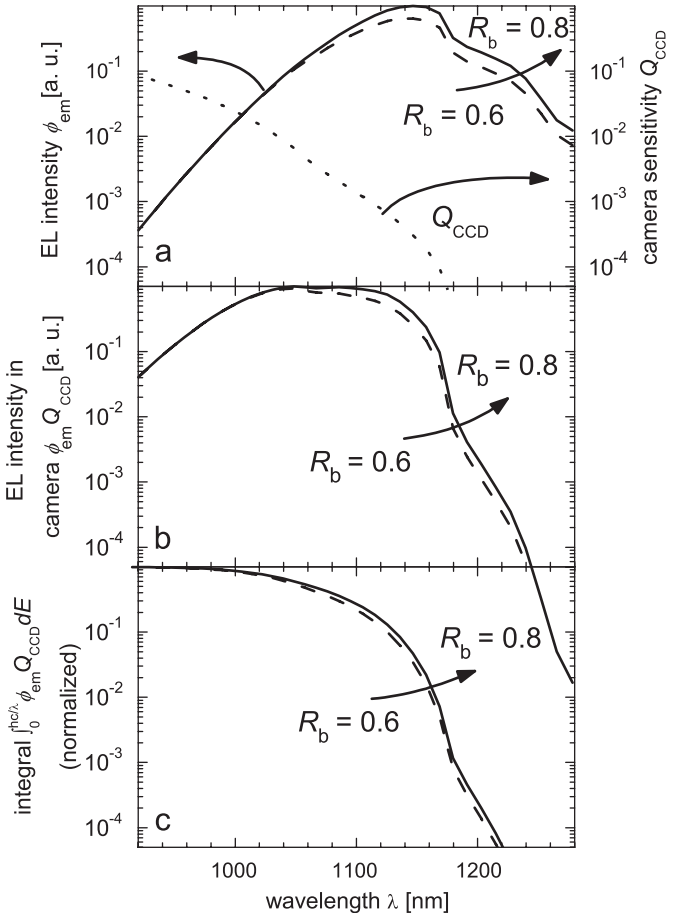

Fig. 6. (a) EL spectra for two back reflectances $R_b = 0.6$ (dashed line) and $R_b = 0.8$ (solid line). The other parameters are $L = 400$ μm, $S = 1000$ cm/s and the thickness $w = 200$ μm. In contrast to Fig. 3a the spectra are now not normalized to the peak. (b) Multiplication of the spectra in (a) with the camera sensitivity in (a). (c) Result of solving the integral $\int_0^{hc/\lambda_{cut}} \phi_{em} Q_{CCD} dE$ as a function of λ_{cut} and normalizing it to the integral over the whole spectrum.

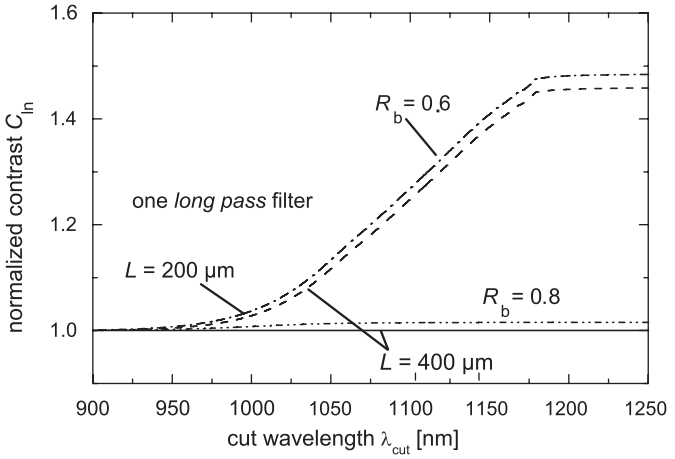

Fig. 7. Normalized contrast for the case of a long-pass filter with varying cut wavelength. In this case, different values of the back surface reflectance R_b lead to a pronounced contrast for cut wavelengths $\lambda_{cut} > 1150$ nm whereas different values of the effective diffusion length L_{eff} have no influence.

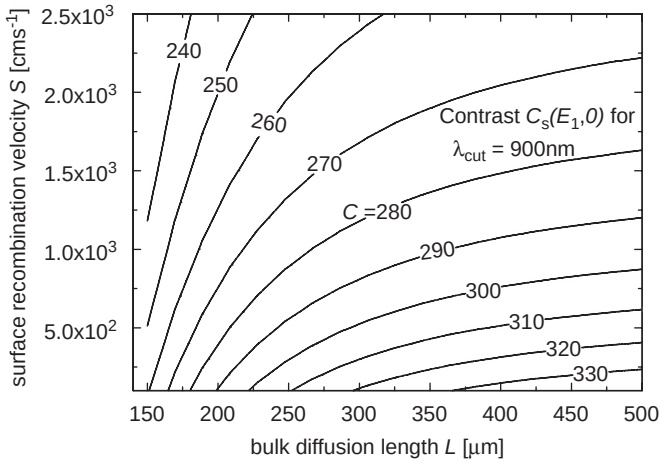

Fig. 8. Possible combinations of surface recombination velocity S and diffusion length L that lead to a certain contrast when applying a short-pass filter with a cut wavelength $\lambda_{cut} = 900$ nm.

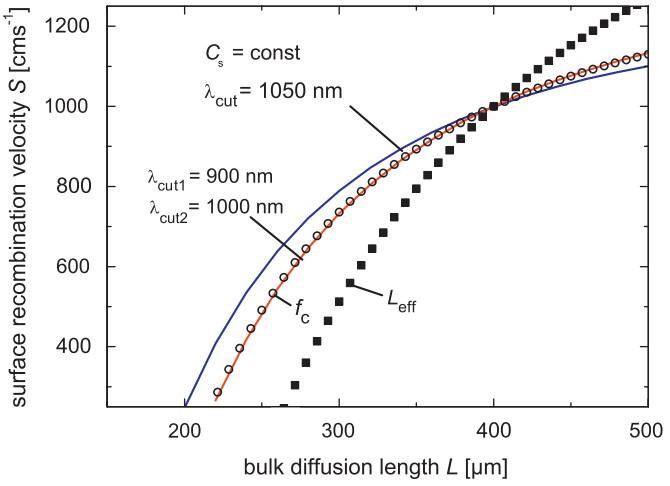

Fig. 9. Lines of equal L_{eff} and $\overline{f_c}$ for the case of $L = 400\,\mu$m and $S = 1000$ cm/s as well as two lines of equal contrast for two different combinations of short-pass filters. Independent determination of S and L is more difficult with EL than with quantum efficiency measurements since the angle between the curves with different filters is much smaller than the one between L_{eff} and $\overline{f_c}$.

variations of both S and L are possible. Only for high quality bulk material ($L \gg w$), S is determined accurately.

The question remains, whether a combination of measurements can help us to distinguish between recombination in the bulk and at the surface. For quantum efficiency measurements this is possible, when comparing the first and second linear regime in Fig. 1 [11,12]. The first linear regime gives information about L_{eff}, while the spectral region for longer absorption lengths depends on the average collection probability

$$\overline{f_c} = \frac{1}{w}\int_0^w f_c(x)\,dx = \frac{L}{w}\frac{S(\cosh(w/L)-1)+D/L\,\sinh(w/L)}{S\,\sinh(w/L)+D/L\,\cosh(w/L)}. \quad (14)$$

For high absorption lengths, the photogeneration becomes uniform and the collection probability of the generated charge carriers independent of thickness. The two different combinations of S and L as defined by Eqs. (3) and (13) allow to distinguish S and L if both L_{eff} and $\overline{f_c}$ have an intersection in the (S,L)-plane. A similar approach is in principle possible, combining the EL measured with different filters with each other.

Fig. 9 shows both the intersection of L_{eff} and $\overline{f_c}$ and of the EL with two different combinations of short-pass filters. For the chosen parameter combination $S = 1000$ cm/s and $L = 400\,\mu\text{m} = 2w$, it is difficult to find two filter-combinations that do not lead to nearly parallel curves. Although the intersection is clearly visible in the simulation, for experimental purposes the curves are probably not linearly independent enough. Both EL curves resemble the case for $\overline{f_c}$. Thus, the approach of Bothe et al. [16] to use light beam induced current (LBIC) measurements for getting local values for L_{eff} will lead to clearer results, if the injection level dependence of recombination is not too strong.

5. Summary

In summary, we show how the simulation and understanding of the spectral shape of electroluminescence measurements is simplified by the link between EL emission and solar cell quantum efficiency. Applying our knowledge of quantum efficiency interpretation to the case of EL images helps us to extend the method of Würfel et al. [5] to the cases of textured solar cells as well as to the determination of the quality of light trapping. We use simulations to show how to choose a combination of filters to determine recombination parameters independently of optical parameters and that the result is always a combination of possible values for surface recombination velocity and diffusion length. While investigation of recombination parameters requires short-pass filter, we show that the use of a long-pass filter increases the sensitivity for back-side reflection, while decreasing the sensitivity for the diffusion length. Finally, we discuss possibilities to distinguish between recombination in the surface and the bulk.

Acknowledgment

The authors would like to thank K. Taretto for carefully reading the manuscript.

References

[1] T. Fuyuki, H. Kondo, T. Yamazaki, Y. Takahashi, Y. Uraoka, Photographic surveying of minority carrier diffusion length in polycrystalline silicon solar cells by electroluminescence, Appl. Phys. Lett. 86 (2005) 262108-1–262108-3.
[2] K. Ramspeck, K. Bothe, D. Hinken, B. Fischer, J. Schmidt, R. Brendel, Recombination current and series resistance imaging of solar cells by combined luminescence and lock-in thermography, Appl. Phys. Lett. 90 (2007) 153502-1–153502-3.
[3] D. Hinken, K. Ramspeck, K. Bothe, B. Fischer, R. Brendel, Series resistance imaging of solar cells by voltage dependent electroluminescence, Appl. Phys. Lett. 91 (2007) 182104-1–182104-3.
[4] M. Kasemann, M.C. Schubert, M. The, M. Köber, M. Hermle, W. Warta, Comparison of luminescence imaging and illuminated lock-in thermography on silicon solar cells, Appl. Phys. Lett. 89 (2006) 224102-1–224102-3.
[5] P. Würfel, T. Trupke, T. Puzzer, E. Schäffer, W. Warta, S.W. Glunz, Diffusion lengths of silicon solar cells from luminescence images, J. Appl. Phys. 101 (2007) 123110-1–123110-10.
[6] U. Rau, Reciprocity relation between photovoltaic quantum efficiency and electroluminescent emission of solar cells, Phys. Rev. B 76 (2007) 085303-1–085303-8.
[7] T. Kirchartz, U. Rau, M. Kurth. J. Mattheis, J.H. Werner, Comparative study of electroluminescence from Cu(In,Ga)Se_2 and Si solar cells, Thin Solid Films 515 (2007) 6238–6242.
[8] T. Kirchartz, U. Rau, Electroluminescence analysis of high efficiency Cu(In,Ga)Se_2 solar cells, J. Appl. Phys. 102 (2007) 104510-1–104510-8.
[9] T. Kirchartz, U. Rau, M. Hermle, A.W. Bett, A. Helbig, J.H. Werner, Internal voltages in GaInP/GaInAs/Ge multijunction solar cells determined by electroluminescence measurements, Appl. Phys. Lett. 92 (2008) 123502-1–123502-3.
[10] N.D. Arora, S.G. Chamberlain, D.J. Roulston, Diffusion length determination in *p-n* junction diodes and solar cells, Appl. Phys. Lett. 37 (1980) 325–327.
[11] P.A. Basore, Extended spectral analysis of internal quantum efficiency, in: Proceedings of the 23rd IEEE Photovoltaic Specialists Conference, IEEE, New York, 1993, pp. 147–152.

[12] M. Hirsch, U. Rau, J.H. Werner, Analysis of internal quantum efficiency and a new graphical evaluation scheme, Solid State Electron. 38 (1995) 1009–1015.
[13] C. Donolato, A reciprocity theorem for charge collection, Appl. Phys. Lett. 46 (1985) 270–272.
[14] J. Mattheis, Mobility and homogeneity effects on the power conversion efficiency of solar cells, Ph.D. Thesis, University of Stuttgart, 2008, p. 140.
[15] 〈http://www.pco.de/download/?url = %2Fdata%2FBR_SCQEE_0505.pdf〉.
[16] K. Bothe, D. Hinken, K. Ramspeck, B. Fischer, R. Brendel, Combined quantitative analysis of electroluminescence images and LBIC mappings, in: Proceedings of the 22nd European Photovoltaic Solar Energy Conference in Milan, WIP Renewable Energies, Munich, 2007, pp. 1673–1677.